Comments to the Author:

Dear Mansur Ali Jisan ,

let me suggest to slightly rephrase your text:

"The increase in storm surge level for TC Aila in Charchanga station is significantly higher than what we found in the Barisal station (Table 6). This difference is likely due to the different role played by the topography and bathymetry near the two stations and their coarse resolution in model grid. In absence of a strong interaction with the bottom topography, the increase in peak water level during the hurriccanes should approximately match the mean SLR. However, both Charchanga and Barisal are located away from the open water, and thus the complex topography and bathymetry play a role in regulating water levels in a complex way. The large simulated storm surge level increase for TC Aila at the Charchanga station may be unrealistic and in our opinion it is an artificial effect due to coarse resolution of the model grid near the station. "

Obviouly feel free changing it.

Otherwise, if you agree, please submit a new version with these new phrasing.

Best regards,

Piero

Dear Dr. Piero Lionello,

Thank you for the suggestions. We agree with what you mentioned. We've updated the text accordingly.

Best Regards,

Mansur

Ensemble Projection of the Sea Level Rise Impact on Storm Surge and Inundation in the Coastal Bangladesh

Mansur Ali Jisan[1], Shaowu Bao[1], Leonard J. Pietrafesa[1]
[1]Department of Coastal and Marine Systems Science, Coastal Carolina University, Conway, South Carolina, United States.

Correspondence to: Mansur Ali Jisan (mjisan@g.coastal.edu)

Abstract.

The hydrodynamic model Delft3D is used to study the impact of Sea Level Rise (SLR) on storm surge and inundation in the coastal region of Bangladesh. To study the present-day inundation scenario, the tracks of two known tropical cyclones (TC) were used: Aila (Category 1; 2009) and Sidr (Category 5; 2007). Model results were validated with the available observations. Future inundation scenarios were generated by using the strength of TC Sidr, TC Aila and an ensemble of historical TC tracks but incorporating the effect of SLR.

Since future change in storm surge inundation under SLR impact is a probabilistic incident, that's why a probable range of future change in inundated area was calculated by taking into consideration the uncertainties associated with TC tracks, intensities and landfall timing.

The model outputs showed that the inundated area for TC Sidr, which was calculated as 1860 km^2, would become 31% higher than the present-day scenario if a SLR of 0.26 m occurs during the mid-21st-century climate scenario. Similar to that, an increasing trend was found for the end-21st-century climate scenario. It was found that with a SLR of 0.54 m, the inundated area would become 53% higher than the present-day case.

Along with the inundation area, the impact of SLR was examined for the changes in future storm surge level. A significant increase of 14% was found in storm surge level for the case of TC Sidr in Barisal station if a SLR of 0.26 m occurs in the mid-21st-century. Similar to that, an increase of 29% was found in storm surge level with a SLR of 0.54 m in this location for the end-21st-century climate scenario.

Ensemble projections based on uncertainties of future TC events also showed that, for a change of 0.54 m in SLR, the inundated area would range between 3500-3750 km^2 whereas for present-day SLR simulations it was found within the range of 1000-1250 km^2

These results revealed that even if the future TCs remain at the same strength as at present, the projected changes in SLR will generate more severe threats in terms of surge height and the extent of inundated area.

1. Introduction

In addition to routine inundation from upstream river water and the downstream tides, the coastal part of Bangladesh is frequently flooded by storm surges induced by tropical cyclones (TCs). Typically, TC-induced storm surges in this area initiate in the central or southern part of the Bay of Bengal or near the Andaman Sea. TCs normally occur during April – May, the pre-monsoon period, and again from October – November, the post monsoon period. Harris (1963) mentioned that five basic processes (i.e., pressure, direct wind, earth's rotation, waves and rainfall effects) cause water level rise under storm conditions. Pietrafesa *et al.* (1986) also pointed out that high water at the mouths of coastal estuaries, bays, and rivers can block discharges of upstream waters and contribute to upstream flooding; a non-local effect. Among these processes, storm surges form primarily due to the TC wind stresses mechanically driving the surface frictional layer onshore. Assuming an idealized balance between pressure gradient force and surface wind stress with assumed small bottom stress, the surge related to TC wind stress can be expressed as $\Delta\eta = \frac{\tau_w L}{g\rho h}$, where L is the fetch of the wind (the distance over which the wind blows), τ_w is the wind stress due to the friction between the moving air and water surface, g is the gravity, ρ is the density of water, h is the depth near the coast (Hearn, 2008). Also, as a secondary process, due to the differences in pressure level, the water level rises in the areas of low atmospheric pressure and falls in the areas of high atmospheric pressure, which is how the rising water level offsets the low atmospheric pressure to keep the total pressure constant (Harris, 1963).

According to Murty et al. (1986), the surge amplifies as it approaches the coast due to the shallow continental shelf of the Bay of Bengal and hence it causes massive flooding in the low-lying coastal areas. A large percentage of the Bangladesh population resides in the low-lying coastal regions of the country. Most of the areas near the coastal zone of Bangladesh have been formed by the process of riverine sedimentation and because of that the low-lying areas are relatively flat and as such are susceptible to flooding even under normal astronomical tide conditions. Furthermore, the triangular shape of the Bay of Bengal region makes storm surges more distressing, as a funneling effect occurs. The geomorphological characteristics of the region have made the locales prone to major TC events, events which have occurred multiple times in the past, directly causing loss of lives, property, livelihoods and the economy of the country (Haque, 1997).

Future climate change scenarios may further exacerbate the threats of TC-induced storm surge and inundation. According to the Intergovernmental Panel on Climate Change Fourth Assessment Report (IPCC 4AR), there is a high probability of major changes in TC activity across various ocean basins including the Arabian Sea and the Bay of Bengal. According to Milliman et al. (1989), this Ganges-Brahmaputra-Meghna

Delta region has long been characterized as a highly vulnerable zone due to its exposure to the increasing trend of SLR. According to the SLR analysis done by the South Asian Association for Regional Cooperation based on the 22-year records of observed sea level at Charchanga, Cox's Bazar and Hiron Point, sea level is rising at rates of 6.0, 7.8 and 4 mm/year, respectively in those three locations (SMRC, 2003). These rates are much higher than the global rate of SLR (~ 3.2 mm/year) over the last 25 years (Pietrafesa et al., 2015). Based on Warrick et al. (1996), the sea level in the Bay of Bengal is also influenced by local factors including tectonic setting, deltaic processes, and sediment load; for example, the coastal region of Bangladesh has been subsiding due to the pressure on the Earth's crust from the sediment with thick layers that have formed over millions of years. Warrick et al. (1996) also analyzed the recent history of land accretion and suggested that the subsidence is also balanced by land accretion due to sediment supply from the coast. These physical phenomena have been shaping the coast of Bangladesh over the past 100 years. A global SLR of 26-59 cm has been projected over the next 84 years to 2100 by the IPCC under the scenario A1F1 (Meehl et al. 2007). In this proposed work, we will use the SLR projections from Caesar et al. (2017; under review), which is based on IPCC AR5 and suggests a projection of SLR of 26 cm for the mid-21st-century (2040 -2060) and 54 cm for the end-21st-century (2079 -2099).

Previous studies have analyzed the likely impact of climate change, especially SLR, on storm surge and inundation in this region. Using hydrodynamic models, Ali (1992) showed that with an increase of 1.0 and 1.5 m of SLR, 10% and 15.5%, respectively, of the entirety of Bangladesh would get flooded under the strength of future TCs. Karim and Mimura (2008) used a 1-D hydrodynamic model to study the inundation under several scenarios of climate and for the case of future TCs by changing sea surface temperature, SLR, wind speed and sea level pressure. Based on their results, Karim and Mimura (2008) concluded that with an increase of 2°C in SST and 0.3 m of SLR, the flood risk area would be 15.3% more than the present-day risk area and the depth of flooding would increase by as much as 22.7% within 20 km from the coastline. Both Ali (1992) and Karim & Mimura (2008) considered SST rise and future strength of TCs in simulating the future storm surge and inundation.

However, the impacts of climate change on the frequency and intensity of TCs are still debatable (Knutson *et al*., 2010). The projection of the TC characteristics in the Bay of Bengal region is unclear as well. To improve these uncertainties, a reasonable method to examine the impact of future SLR on storm surge and inundation would be to construct an ensemble of tracks and intensities of possible land-falling TCs along the Bangladesh coast based on the historical TC records. From this statistical approach, we can quantify the probable impact of TC tracks under future SLR change. To date, such an approach has not been done and will be the method of this study.

We first use Delft3D to simulate the present-day storm surge and inundation using the strength of two recent TCs (Sidr and Aila) and validate the simulations with observational data. Future storm surge and inundation scenarios were then generated by incorporating the projected SLR.

The study was carried out in the Ganges-Brahmaputra-Meghna Delta regions (Figure 1a). According to Integrated Coastal Zone Management Plan, 19 districts of Bangladesh located near the Bay of Bengal area were defined as the coastal areas. We've considered all those in this study. We selected two TC cases in this study, a strong Saffir-Simpson(SS) Category-5 that directly hit the study area, TC Sidr, and the other a Category -1 storm that made landfall in the southwest part of the study domain, TC Aila.

TC Sidr made landfall near Barguna district (Figure 1a) in 2007, causing ~ 3000 human fatalities and leaving millions homeless. This Category-5 cyclone is considered one of the most powerful cyclones in the past 15 years to have made landfall in Bangladesh, which affected over nine million people living in the Bangladesh coastal areas. The districts of Patuakhali, Khulna, Barguna and Jhalokathi were badly affected. During TC Sidr, around 15% of the affected people took refuge in nearby cyclone shelters. In the village of Angul Kata in Barguna district, around 1500 people took shelter in eight reinforced pillars to protect themselves from the tidal surge of around 5 m. If there had been no shelters, the death toll could have reached into the hundreds in that area.

The other cyclone studied in this paper, TC Aila (Figure 1a) occurred in the Bay of Bengal region in 2009. Although a Category-1 storm, Aila caused ~ 190 deaths and affected 4.8 million people, the devastation that left a long-term impact. The locales mainly affected were Khulna, Patuakhali and Chandpur. The storm surge due to Aila broke a dam in Patuakhali and submerged five villages, destroying a huge number of homes and leaving thousands of people homeless. Most of the people living in those affected areas took shelter in the nearest cyclone shelters. According to government sources, approximately 2,500,000 houses had been destroyed completely and 3,700,000 houses had been damaged.

The structure of the paper is as follows: brief description of the Delft3D Flow model and the methodologies used to simulate future changes in storm surge and inundation, to generate ensemble projections of storm surge inundation are discussed in section 2. In section 3, validation of the model results, present-day storm surge inundation scenarios, ensemble projection of storm surge inundation and future change in storm surge level [1]are presented. Section 4 includes discussion of model results and the uncertainties associated with the future projections. Finally, section 5 presents the concluding remarks on research findings.

[1] In this paper, the storm surge results refer to the total water level including both normal tides and the water level change due to storm.

2. Methodology

2.1 Modeling Methodology

2.1.1 Application of Numerical Model

To develop the present-day and future inundation scenario in the coastal regions of Bangladesh, the Delft3D-FLOW (Delft Hydraulics, 2006), a multidimensional (2D or 3D) hydrodynamic and transport simulation program that calculates non-steady flow and transport phenomena resulting from tidal and meteorological forcing was used. Delft3D-FLOW solves the unsteady shallow water equation in two (depth-averaged) or three dimensions. The system of equations consists of the horizontal equations of motion, the continuity equation, and the transport equations for conservative constituents. The equations are formulated in orthogonal curvilinear coordinates or in spherical coordinates. Delft3D – FLOW module's two-dimensional, depth averaged flow equations can be applied for modeling tidal waves, storm surges, tsunamis, harbor oscillations (seiches) and transport of pollutants in vertically well-mixed flow regimes. In this paper Delft3D's 2D mode for barotropic depth-integrated flow has been applied. The equations are listed below.

$$\frac{\partial \zeta}{\partial t} + \frac{1}{\sqrt{G_{\xi\xi}\sqrt{G_{\eta\eta}}}} \frac{\partial\left[(d+\zeta)u\sqrt{G_{\eta\eta}}\right]}{\partial \xi} + \frac{1}{\sqrt{G_{\xi\xi}\sqrt{G_{\eta\eta}}}} \frac{\partial\left[(d+\zeta)v\sqrt{G_{\xi\xi}}\right]}{\partial \xi} = Q \quad (1)$$

$$\frac{\partial u}{\partial t} + \frac{u}{\sqrt{G_{\xi\xi}}}\frac{\partial u}{\partial \xi} + \frac{v}{\sqrt{G_{\eta\eta}}}\frac{\partial u}{\partial \eta} + \frac{uv}{\sqrt{G_{\xi\xi}}\sqrt{G_{\eta\eta}}}\frac{\partial \sqrt{G_{\xi\xi}}}{\partial \eta} - \frac{v^2}{\sqrt{G_{\xi\xi}\sqrt{G_{\eta\eta}}}}\frac{\partial \sqrt{G_{\eta\eta}}}{\partial \xi} - fv + \frac{g}{\sqrt{G_{\xi\xi}}}\frac{\partial \zeta}{\partial \xi} = -\frac{1}{\rho_0\sqrt{G_{\xi\xi}}}\frac{\partial P_{atm}}{\partial \xi} + F_\xi \quad (2)$$

$$\frac{\partial v}{\partial t} + \frac{u}{\sqrt{G_{\xi\xi}}}\frac{\partial v}{\partial \xi} + \frac{v}{\sqrt{G_{\eta\eta}}}\frac{\partial v}{\partial \eta} + \frac{uv}{\sqrt{G_{\xi\xi}}\sqrt{G_{\eta\eta}}}\frac{\partial \sqrt{G_{\xi\xi}}}{\partial \eta} - \frac{u^2}{\sqrt{G_{\xi\xi}\sqrt{G_{\eta\eta}}}}\frac{\partial \sqrt{G_{\xi\xi}}}{\partial \eta} + fu + \frac{g}{\sqrt{G_{\xi\xi}}}\frac{\partial \zeta}{\partial \xi} = -\frac{1}{\rho_0\sqrt{G_{\eta\eta}}}\frac{\partial P_{atm}}{\partial \eta} + F_\eta \quad (3)$$

where ξ, $\boldsymbol{\eta}$ are the spatial coordinates, ζ is representing water level above some horizontal plane of reference (m), u and v are the velocities in the ξ and $\boldsymbol{\eta}$ direction (m/s), d is the water depth below some horizontal plane of reference (m), f is the Coriolis forcing due to the rotation of the earth, g is the acceleration of gravity (m/s^2), P_{atm} is the atmospheric pressure at water surface (kg/m/s^2), Q is the discharge of water, evaporation or precipitation per unit area (m/s) , $\boldsymbol{\rho}_0$ is the the density of water, $\sqrt{G_{\xi\xi}}$ is the coefficient used to transfer one coordinate system into another one (m), F_ξ is the turbulent momentum flux in ξ-direction (m/s^2), $F_{\boldsymbol{\eta}}$ is the turbulent momentum flux in $\boldsymbol{\eta}$-direction (m/s^2). Along with the appropriate set of initial and boundary conditions, the above-mentioned equations have been solved on an Arakawa-C type finite

difference grid. Delft3D- FLOW manual (Delft Hydraulics, 2006) contains detailed information about these numerical aspects.

2.1.2 Model Grid and Bathymetry

The grid was set up using spherical coordinates. The grid spacing varies from a minimum of 125 m to a maximum of 1140 m. The finer resolution was applied over land for calculating the inundation or wetting process accurately.

In this study, the land topography data were obtained from NASA's Shuttle Radar Topography Mission (SRTM) 90-m resolution datasets (Figure 1b). The bathymetries of the rivers and estuaries are specified using the cross sections measured by the Institute of Water and Flood Management, Bangladesh. The ocean bathymetry was specified using the data from the General Bathymetric Chart of the Oceans 30-arc-sec interval gridded data (BODC, 2003, Figure 1b). Bathymetry and topographic data were interpolated over the model domain using triangular interpolation and grid-cell averaging methods of Delft3D (Delft Hydraulics, 2006).

2.1.3 Wind and Pressure Field

Track data of TCs Sidr and Aila were obtained from the Indian Meteorological Department (www.imd.gov.in). Using those data as input, TC surface winds and mean sea level pressure fields were generated using the Wind Enhancement Scheme (WES) (Heming et al. 1995) method based on the analytical equation by Holland (1980). Delft3D slightly improved the original WES by introducing TC asymmetry. Unlike some previous method that incorporates TC wind asymmetry information from observations (Xie et al. 2006), in WES the asymmetry was brought about by applying the translation speed of the cyclone center displacement as steering current and by introducing rotation of wind speed due to friction (Delft Hydraulics, 2011,Heming et al. 1995).

According to the Holland's equation, gradient wind speed $V_g(r)$ at a distance r from the Centre of the cyclone is expressed as the following:

$$V_g(r) = \left[\frac{AB(p_n - p_c)\exp\left(-\frac{A}{r^B}\right)}{\rho r^B} + \frac{r^2 f^2}{4}\right]^{0.5} - \frac{rf}{2} \quad (4)$$

Here ρ is the density of air, p_c is the central pressure and p_n is the ambient pressure, the Coriolis parameter is represented by f . A and B are determined empirically; with the physical meaning of A as the relation

of pressure or wind profile relative to the origin, and parameter B defining the shape of the profile. Delft3D introduces a central pressure drop of $p_d = p_n - p_c$. By equating $\frac{dV_g}{dr} = 0$, and assuming f=0 in the region of maximum winds where the Coriolis force is small compared to the pressure gradient and centrifugal forces, the radius of maximum winds R_w can be given as follows:

$$R_w = A^{1/B} \quad (5)$$

Thus, R_w is independent of the relative values of ambient and central pressure and is defined entirely by the scaling parameters A and B. Substitutions lead to the expression for the maximum wind speed V_m

$$V_m = \left[\frac{Bp_d}{\rho e}\right]^{0.5} \quad (6)$$

Where *e* is the base of the natural logarithm (=2.71828182846).

Complete details about this method can be found in the user manual of Delft3D Flow (Delft Hydraulics, 2006), Holland (1980), and Vatvani et al. (2002).

The circular grid of TC wind fields used in this study consists of 36 columns and 500 rows and the data were updated at 6 hourly intervals throughout its movement until the landfall. Figure 2 shows a snapshot of the wind field of TC Sidr over the model domain, before landfall, generated using Holland's equation above.

2.1.4 Roughness

The spatially varying Manning's Roughness value was defined based on land cover, such as vegetation, rivers, and ocean (Table 1). In the study domain, a mangrove forest, Sundarbans, is located in the Southwest region, near TC Sidr's landfall location (Figure 1a). Sakib et al. (2015) found that Sundarban plays a significant role as a buffer in reducing the total inundation during TC passages. Therefore, in this study, the mangrove region was considered. In selecting the roughness values, methods described in Zhang et al. (2012) were followed and slightly modified values were defined for the study area based on the vegetation types in that area.

2.1.5 Boundary conditions

Upstream boundaries were specified as discharges at the mouths of the three major rivers; the Ganges, the Brahmaputra & the Upper Meghna; obtained from the Bangladesh Water Development Board (BWDB) as

daily discharge. The downstream ocean boundary was defined by the Topex/Poseidon Inverse Tidal model, based on Egbert et al. (1994). Location of the downstream ocean boundary is shown in Figure 1a.

2.2 Calculation Procedure for Present-day and Future Storm Surge and Inundation Scenario

To generate storm surge and inundation for present-day climate scenario, upstream discharge and downstream water level data from the present-day were used. For future SLR scenarios, present-day hydrodynamic conditions and the strengths of present-day TCs were used but the future sea level was modified based on the SLR projections by Caesar et al. *(2017; under review)*. Scenarios were generated for both the mid-21st-century and the end-21st-century time horizons for these TCs, Sidr and Aila. Finally, comparisons were made in terms of storm surge and inundation to identify the changes between present-day and future SLR scenarios.

Now, future storm surge inundation due to SLR is a probabilistic event that requires proper addressing of the uncertainties associated with the input parameters. To address the future tropical cyclone uncertainties and obtain statistically significant results, we created an ensemble of tropical cyclone tracks. The ensemble tracks were generated from different historical tropical cyclones that made landfall over the study domain with different intensities (Table 2). Along with the uncertainties associated with future landfall locations, the intensity of Sidr-like and Aila-like TCs may be different. So, to address the uncertainty with the intensity, we increased and decreased their intensity by 10% to simulate a probable range of future storm surge inundation.

Storm surge inundation can also be different based on landfall timing. If a storm made landfall during the high astronomical tide condition, its flooding would have been much higher at that time than what could happen during a low astronomical tide condition. For example, the tides shown in Figures 3 and 7 as the water level oscillations have amplitudes as high as 3 m, which could significantly affect the extension of flooded area, depending on whether the storm's landfall coincides with a high tide or a low tide. We note that TC Sidr and TC Aila made landfall during the high tide conditions, which may not always be applicable for the future TCs. To also address uncertainties with the TC landfall timing, experiments were conducted by changing the timing of landfall to identify the impact of high tide and low tide on storm surge and inundation. The change of timing in these tide-related experiments was implemented by modifying the tracks of the storms so that their landfalls coincide with a high tide, a tide, or a zero-tide condition, in addition to their actual tidal phases. Here in this study, future storm surge inundation scenarios caused by the ensemble tracks will then be simulated by incorporating the projected SLR. By taking all these parameters into consideration, we conducted a total 108 ensemble simulations (36 for each; present-day

and two SLR scenarios). Parameters that were considered in making ensemble projections are shown in Table 3.

3. Results

3.1 Validation of the Model

Hourly tidal data from the Bangladesh Inland Water Transport Authority (BIWTA) was used to evaluate the performance of the model used in this study. The model simulation's root mean square error (RMSE)[7], mean absolute error (MAE)[8] and dimension-less Nash-Sutcliffe coefficient (E)[9] (Nash and Sutcliffe, 1970) were calculated and listed in Table 4. A Nash-Sutcliffe coefficient ranges between negative infinity (no skill simulation) and one (perfect simulation).

$$\boldsymbol{RMSE} = \sqrt{\frac{\sum_{i=1}^{n}(X_{obs,i}-X_{model,i})^2}{n}} \quad (7)$$

$$MAE = \frac{1}{n}\sum_{i=1}^{n}\left|X_{obs,i} - X_{model,i}\right| \quad (8)$$

$$E = 1 - \frac{\sum_{i=1}^{n}(X_{obs,i}-X_{model})^2}{\sum_{i=1}^{n}(X_{obs,i}-\overline{X_{obs}})^2} \quad (9)$$

The simulated water levels were compared against the measured data from BIWTA at two locations: Barisal and Charchanga (Figure 1a). Barisal station is located more towards the inland whereas Charchanga is located near the coastline where the grid cell resolution was coarse. But none of them are in the open ocean water, which is important to get a clear idea about storm surge level. TC Sidr made landfall near the Barisal Station (Figure 1a) and the impact of the storm surge was clearer at the Barisal station than that of TC Aila, which made landfall outside the model domain (Figure 1a); therefore, its impact was not as clear as that of Sidr.

In Figure 3(a) for TC Sidr at the Barisal station, the modeled water level, including storm surge and astronomical tides, was slightly lower than the observations, and at the Charchanga station (Figure 3b) the measured water level variation displayed smaller amplitudes than did the model outputs for positive tides, larger amplitudes than the modeled water level for negative tides, perhaps due to the coarse resolution of bathymetry. Similar types of variations between measured and modeled water level were found for TC Aila (Figure 3c and Figure 3d). Nevertheless, the modeled water level variations during TCs Sidr and Aila agreed reasonably well with measured data; as also confirmed by the calculated RMSE, MAE and Nash-Sutcliffe coefficient (Table 4). Therefore, we conclude that the method can be used to study the impact of SLR on storm surge and inundation in future climate change scenarios.

3.2 Present-day Inundation Scenario

The storm surge inundation scenarios due to the two TCs considered are shown in Figure 4. It can be seen from Figure 4 that the area flooded by TC Sidr (yellow shade+red shade) was much higher than the area flooded by TC Aila (white shade+red shade), a result that is consistent with the fact that the category-5 TC Sidr was much stronger than the category-1 TC Aila and directly hit the study area. The maximum sustained wind speed for TC Sidr was 260 km/h whereas for TC Aila it was 110 km/h. The landfall location of Sidr was on the Eastern side of Sundarban, while for Aila, the landfall location was towards the Western side of Sundarbans. That explains why the inundations due to TC Sidr were located near the eastern side of Sundarban, whereas for Aila, the inundation was located mainly in the western part. The extent of inundation due to Sidr (1860 km^2) was 54% larger than that of Aila (1208 km^2)

Sakib et al. (2015) showed that Sundarban acted as a buffer zone in reducing the impact of Sidr and thereby reduced much of the potential inundation depth and extent of flooding. As mentioned before, in the model simulation the impact of Sundarban was realized using a higher Manning's roughness value as resistance for the surge to travel.

3.3 Impact of Future Climate Scenarios on Storm Surge Inundation

Future inundation scenarios were generated for two different time horizons: one for the mid-21st-century and the other for the end-21st-century. The initial ocean water level was raised by 0.26 m and 0.54 m for the mid-21st-century and end-21st-century, respectively. The upstream river discharge and downstream ocean water level were used from present-day climate scenarios.

In this section we seek to answer the question: if present-day's TCs were to happen in future SLR scenarios, what storm surge and inundation hazard would they cause? Therefore, the tracks and intensities of the two present-day TCs, Sidr and Aila, were used as the model wind input parameters.

The model simulated inundated areas and the percent variations were shown in Table 5 and Figure 5. Figure 5 shows that under future SLR scenarios, the inundated areas caused by TCs Sidr and Aila would be significantly higher than those under the present-day climate condition, as indicated by the white color shaded areas. For the category-5 TC Sidr, the inundated area would be 31% (2437 km^2) and 53% (2846 km^2) higher than present-day's 1860 km^2 inundated area, in mid-21st-century (0.26 m SLR) and end-21st-century (0.54 m SLR) climate scenarios, respectively (Figure 5a and Figure 5b)

Similarly, for the category-1 TC Aila, there would be an increase in inundated areas. The simulated inundated areas for TC Aila under mid-21st-century and end-21st-century were 1550 km^2 (28%) and 1770 km^2 (47%), respectively (Figure 5c and Figure 5d) whereas for the present-day scenario it was found to be 1208 km^2.

However, in Figure 5, there are several small areas of yellow color indicating zones flooded under present conditions but not flooded during future SLR conditions. This is because Figure 5 showed snapshots of the inundation conditions at one particular time. Some areas may experience alternating wetting and drying conditions, which may explain why some areas are flooded with present SLR and not with higher SLR: this is so only at that particular time. The authors expect that those areas are flooded at other times.

All these simulations were carried out using the present-day tides, upstream river discharges and TC tracks and strengths, with only the initial sea water level raised to reflect the effect of the projected future SLR. Therefore, the results suggest that even if the future TCs strengths, tides, and river discharges remain the same as in the present-day climate condition, future SLR would significantly increase the inundated area, by as high as 53%.

3.3.1 Ensemble Projection of Future Storm Surge Inundation under SLR Conditions

As discussed in section 2.2, the future change in storm surge inundation can be different based on the intensity, landfall location and timing of future TCs. By considering all these uncertainty factors mentioned in Table 3, a column plot was created (Figure 6) for present-day sea level and future SLR scenarios. Ensemble simulation outputs also showed an evident increase in the inundated area under the effect of SLR. For the present-day scenario (black column), out of 36 simulations, frequency of storm surge inundation incidents that would likely occur between the range of 1000-1250 km^2 is 13. whereas for 0.26 m of SLR(red column), peak of the column shifted towards right side with a maximum frequency of inundation events occurred within the range of 2000-2250 km^2 (10 times out of 36 simulation results). And for 0.54 m of increase in sea level (blue column), the peak of the column shifted more towards the right and the maximum number of simulation outputs (11 out of 36 simulations) showed the range of inundation to be within 3500-3750 km^2. These results show that even the change in intensities of future TCs are indefinite and the landfall timing is uncertain, increase in sea level is going to increase the area of inundation.

3.4 Impact of Sea Level Rise on Future Storm Surge Level

In addition to the inundation area, SLR would also greatly affect storm surge levels. Similar to the approach used in the inundation study (Section 3.3), TCs Sidr- and Aila-induced storm surges in the future SLR scenarios were simulated using their recorded strengths.

The simulated storm surge water levels in future SLR scenarios were compared with both the observed and model generated ones under the present-day scenarios (Figure 7). It is to be mentioned that, while generating the future water level under the effect of SLR, the baseline was only changed by considering the SLR effect and based on that factor the future storm surge level was calculated. Other than that, the water level is the same as present-day TCs.

From Figure 7a and Table 6 we can see that for the case of TC Sidr the simulated storm surge level would become 2.13 m in Barisal station which is around 14% higher than the present-day scenario. Similar to that, under the end-21st-century 0.54 m SLR scenario in Barisal, the storm surge would be around 29% higher than the present-day scenario and the peak water level would reach 2.41 m.

Increase in storm surge was found at the Charchanga station also. For TC Sidr, under the mid-21st-century scenario (0.26 m SLR), the model simulated storm surge level was found to be 14% higher (1.87 m) than the present-day and 34% higher (2.19 m) (Figure 7b, Table 6) than the present-day for the end-21st-century (0.54 m SLR) climate scenario. It is to be noted that, a slight phase shift in the model simulation occurred at this station from November 13 to November 15. This could happen due to the presence of seiche. However, for rest of the period, phase variations are similar to the observed ones.

For TC Aila in Barisal, under the mid-21st-century SLR scenario the storm surge would become 22% higher (1.58 m) than the present-day, which was 1.29 m (Figure 7c, Table 6). During the end-21st-century climate scenario, the increment would become even higher as the SLR would be 0.54 m. Storm surge under the 0.54 m end-21st-century SLR condition would be 52% higher (1.96 m) than the present day.

At Charchanga, the storm surge would be higher than the present-day condition for TC Aila. Under the 0.26 m mid-21st-century SLR scenario, the storm surge would become 3.07 m which is 23% higher than the present-day condition (Figure 7d, Table 6). And for end-21st-century, this would become 55% higher (3.87 m) than the present day.

To analyze the linearity/non-linearity of storm surge level with respect to SLR, we conducted additional experiments based on 5 SLR scenarios; present-day sea level, 0.26 m of SLR, 0.33 m of SLR, 0.4 m of SLR, 0.47 m of SLR, 0.54 m of SLR, respectively. Results from these experiments are presented in Table 6.

For the case of TC Sidr in Barisal and Charchanga stations, storm surge level increased almost linearly with respect to the addition of water due to the effect of SLR. For example, with a SLR of 0.47 m, the percentage increases in storm surge level with respect to the SLR scenarios in Barisal and Charchanga stations were 96% and 94% m, respectively (Table 6). On the other hand for the case of TC Aila, with a SLR of 0.26 m, the increases in storm surge level were found 112% and 219% respectively for the Barisal and Charchanga station (Table 6). The increase in storm surge level for TC Aila in Charchanga station is significantly higher than what we found in the Barisal station (Table 6). This difference is likely due to the different role played by the topography and bathymetry near the two stations and their coarse resolution in model grid. In absence of a strong interaction with the bottom topography, the increase in peak water level during the TCs should

approximately match the mean SLR. However, both Charchanga and Barisal are located away from the open water, and thus the complex topography and bathymetry play a role in regulating water levels in a complex way. The large simulated storm surge level increase for TC Aila at the Charchanga station may be unrealistic and in our opinion, it is an artificial effect due to coarse resolution of the model grid near the station.

4. Discussions

In this paper, we showed that even if the future TCs keep the same strength like the present-day ones their impact will be much higher in a changing climate due to the effect of SLR. Several other factors not included in the modeling could make the storm surge and inundation situation far worse than that shown in the modeling result. These factors include mangrove coverage decrease, morphological changes, TC strength increase, and upstream river discharge changes.

For including the effect of future SLR in the model simulations, several methodologies were examined. One of the methods with which we experimented in this study was to include the increased sea level in open ocean boundary instead of adding it in to the whole ocean depth by keeping the coastline fixed. This method was used by some previous studies (Pickering et al. 2012). However, in such a case, an additional pressure gradient force was found acting towards the coast which made the inundated area much higher. Therefore, this method was not used in this study. Instead, in this study, the future SLR was added to the whole ocean domain depth.

To make the future SLR simulation realistic, we considered the increased sea level in ocean bathymetry and increased the depth by 0.26 and 0.54 m, respectively, by considering land submergence near the coast. In that case, the result looked much more realistic than the previous one and this is the method we followed in this paper. For example, for the case of TC Aila under the end-21st-century scenario where we used a SLR of 0.54 m SLR at the open ocean boundary instead of adding it to ocean depth and using the hydrodynamic conditions from the present day, the total inundated area was found to be 79% higher than the present-day one. Similar to that, for the mid-21st-century scenario (a 0.26 m SLR), the inundated area was found to be 69% more than the present-day scenario. But when we added the SLR in ocean depth, the mid-21st-century and end-21st-century inundated area were found to be 28% and 47% higher than the present-day scenario. This increase in inundated area was much less than the one that we found by adding the SLR in the open ocean boundary. Figure 8 displays the differences in the inundated area based on the consideration of SLR in the model input.

As discussed earlier, TC Sidr made landfall near Sundarban, where the mangrove forest zone acted as a buffer in reducing the impact of the storm surge flood. That is why, even though it was a TC 5, its impact was not as high as it might have been expected to be. In this study, the roughness of the mangrove forest zone on the South-West part of Bangladesh was considered to be fixed for the present-day as well as for future scenarios. But Mukhopadhyay et al. (2015) predicted that 17% of the total mangrove cover could

disappear by 2105. If this decreasing trend of vegetation were considered in this study, the flooded area could be much higher.

Morphological changes were not considered in this study. But according to Goodbred et al. (2003), each year the eastern, central and western estuaries lose land at a rate of 0.13 cm/year, 0.16 cm/year and 0.16 cm/year, respectively. This could also lead to increased inundated areas for future scenarios. But as the focus of the paper is to estimate the future scenario of storm surge and inundation due to the effect of SLR and to compare with the present-day scenarios, it is important that we keep the roughness and morphological changes constant so that consistent comparisons can be made.

Some previous research showed that there could be increases in hurricane strength and landfall probability in the future due to global climate change (Haarsma et al. 2013, Bender et al. 2010, Bengtsson et al. 2007). Though we slightly modified the present-day TC strengths and selected 12 historical TC tracks to reduce landfall uncertainties and to make ensemble projection of future storm surge inundation, strength may be much higher than the ones that we considered for this study. In such case, the devastation could well be much higher under projected SLR conditions, which is very alarming

In this paper, we used the present-day river discharge data as an upstream boundary for generating future inundation scenarios. But using the INCA-N, an Inland Catchment Modeling system and considering the projected climatic and socioeconomic scenarios, Whitehead et al. (2015) showed that, there would be a significant increase in future monsoon intensities due to the impact of climate change. That would make future flooding scenarios much worse than those experienced presently. So, based on the changes in TC intensity, river discharges, and land-use changes, the situation could well become more badly impacted than what we found in this study.

The findings of our study are important for local governments to consider while they make new management and policy decisions and to improve TC preparedness plans by increasing numbers of shelters and heights. In TC shelters, the first floor should be kept above the high surge waters. Our study showed that, in the future, there would be an increase in surge level from a minimum of 14% up to 55% if a TC 1 or a TC 5 makes landfall under increased SLR conditions (Table 6). So, the authority may consider increasing the height of the first floor considering the future risk of an increase in storm surge level and safety of local populations. Also, our model outputs showed that the inundated area increase would range from 28%-53% (Table 5) if there's any TC 1 or TC 5 was to make landfall with SLRs of 0.26 m or 0.54 m. This shows that a huge number of new areas are going to face the impacts of storm surge inundation and by considering this issue, it is high time to increase the number of TC shelters in the coastal areas of Bangladesh.

5. Conclusion

Employing the Delft3D-FLOW model, we simulated coastal storm surge and inundation for present-day and future SLR scenarios and compared the changes between them. After validating the present-day model, simulations were conducted for mid-21st-century and end-21st-century climate scenarios where the SLR has been considered as 0.26 m and 0.54 m respectively. The model results showed that, with an increase of 0.26 m and 0.54 m SLR, there would be an increase of 31% and 53% of inundated area respectively if TC Sidr was to made landfall with its present-day strength. There would also be an increase of 28% and 47% in inundated area if Category-1 TC Aila would make landfall with its present-day strength but under SLR of 0.26 m and 0.54 m respectively. Outputs from the ensemble projections showed that, even if the TC intensities, landfall location and timings are uncertain, the most probable range of inundated area extent would shift from 1000-1250 km^2 (present day) to 2000-2250 km^2 (under 0.26 m SLR scenario) and 3500-3750 km^2 (under 0.54 m SLR scenario). Besides the inundated area, we also investigated the changes in storm surge level if TC Sidr and TC Aila would make landfall under future SLR conditions. Similar to the inundated area, increases in storm surge levels were found for future scenarios. The significant increase in simulated storm surge and inundation hazards highlights the need for the local governments to improve cyclone preparedness in future SLR scenarios.

Acknowledgement

The authors would like to thank Coastal Carolina University's Cyber-infrastructure project (http://ci.coastal.edu) for providing access to computational resources. Also, we would like to acknowledge Dr. Susan Kay from Plymouth Marine Laboratory, UK for her thoughtful opinions regarding the SLR input in model and Institute of Water and Flood Management, Bangladesh for providing important data and support for this work. The authors also appreciate the helpful comments and suggestions from the three anonymous reviewers. The computation was conducted on the Coastal Carolina University Cyber Infrastructure (CI) project and the National Science Foundation's Extreme Science and Engineering Discovery Environment (XSEDE) project.

References:

Ali, A.: Vulnerability of Bangladesh to climate change and sea level rise through tropical cyclones and storm surges, Climate Change Vulnerability and Adaptation in Asia and the Pacific, Springer, pp. 171–179., doi: 10.1007/978 94-017-1053-4_16, 1996.

Bender, M.A., Knutson, T.R., Tuleya, R.E., Sirutis, J.J., Vecchi, G.A., Garner, S.T., Held, I.M.: Modeled impact of anthropogenic warming on the frequency of intense Atlantic hurricanes, Science, 327, 454–458, doi: 10.1126/science.1180568, 2010.

Bengtsson, L., Hodges, K.I., Esch, M., Keenlyside, N., Kornblueh, L., LUO, J.-J., Yamagata, T.: How may tropical cyclones change in a warmer climate?, Tellus a, 59, 539–561, doi: 10.1111/j.1600-0870.2007.00251.x, 2007.

BODC.: Centenary Edition of the GEBCO Digital Atlas, published on CD-ROM on behalf of the Intergovernmental Oceanographic Commission and the International Hydrographic Organization as part of the General Bathymetric Chart of the Oceans. British oceanographic data centre, Liverpool, 2003.

Caesar, J., Janes, T.,Lindsay, A.: Climate projections over Bangladesh and the upstream Ganges-Brahmaputra-Meghna system, under review, Environmental Science: Processes & Impacts (Under Review), 2017.

Delft Hydraulics.: Delft3D-FLOW user manual. Delft, the Netherlands, 2006.

Delft Hydraulics.:Wind Enhancement Scheme for cyclone modelling, 2011.

Egbert, G. D., Bennett, A. F. and Foreman, M. G. G.: TOPEX/POSEIDON tides estimated using a global inverse model, J. Geophys. Res., 99(C12), 24821–24852, doi:10.1029/94JC01894, 1994.

Goodbred, S.L., Kuehl, S.A., Steckler, M.S., Sarker, M.H.: Controls on facies distribution and stratigraphic preservation in the Ganges–Brahmaputra delta sequence, Sedimentary Geology, 155, 301–316, doi:10.1016/S0037-0738(02)00184-7, 2003.

Haarsma, R.J., Hazeleger, W., Severijns, C., Vries, H., Sterl, A., Bintanja, R., Oldenborgh, G.J., Brink, H.W.: More hurricanes to hit western Europe due to global warming, Geophysical Research Letters, 40, 1783–1788, doi: 10.1002/grl.50360, 2013.

Haque, C.E.: Atmospheric hazards preparedness in Bangladesh: a study of warning, adjustments and recovery from the April 1991 cyclone, Earthquake and Atmospheric Hazards, Springer, pp. 181–202, doi: 10.1007/978-94-011-5034-7_6, 1997.

Harris, D. L.: Characteristics of the hurricane storm surge, Tech. Pap., 48, U. S. Weather Bur., Washington, D. C., 139 pp, 1963.

Hearn, C. J.: The dynamics of coastal models. Cambridge University Press, 2008.

Heming, J. T., Chan, J. C. L. and Radford, A. M.: A new scheme for the initialization of tropical cyclones in the UK Meteorological Office global model, Met. Apps, 2, 171–184, doi:10.1002/met.5060020211, 1995.

Holland, G. J.: An analytic model of the wind and pressure profiles in hurricanes, Monthly weather review, 108(8), 1212-1218, doi:10.1175/1520-0493(1980)108<1212:AAMOTW>2.0.CO;2, 1980.

Karim, M.F., Mimura, N.: Impacts of climate change and sea-level rise on cyclonic storm surge floods in Bangladesh, Global Environmental Change, 18, 490–500, doi: 10.1016/j.gloenvcha.2008.05.002, 2008.

Knutson, T.R., McBride, J.L., Chan, J., Emanuel, K., Holland, G., Landsea, C., Held, I., Kossin, J.P., Srivastava, A.K., Sugi, M.: Tropical cyclones and climate change, Nature Geoscience, 3, 157–163, doi: 10.1038/ngeo779, 2010.

Meehl, G.A., Covey, C., Delworth, T., Latif, M., McAvaney, B., Mitchell, J.F.B., Stouffer, R.J., Taylor, K.E., and. Coauthors,: Global climate projections. Climate Change 2007: The Physical Science Basis, S. Solomon et al., Eds. Cambridge University Press, 2007.

Milliman, John D., James M. Broadus, and Frank Gable.: Environmental and economic implications of rising sea level and subsiding deltas: the Nile and Bengal examples, Ambio, 18 (6), 340-345, doi: , 1989.

Mukhopadhyay, A., Mondal, P., Barik, J., Chowdhury, S.M., Ghosh, T., Hazra, S.: Changes in mangrove species assemblages and future prediction of the Bangladesh Sundarbans using Markov chain model and cellular automata, Environmental Science: Processes & Impacts, 17, 1111–1117, doi: 10.1039/C4EM00611A, 2015

Murty, T.S., Flather, R.A., Henry, R.F.: The storm surge problem in the Bay of Bengal. Progress in Oceanography, 16, 195–233, doi: 10.1016/0079-6611(86)90039-X ,1986.

Nash, J.E., Sutcliffe, J.V.:River flow forecasting through conceptual models part I—A discussion of principles, Journal of hydrology, 10, 282–290, doi:10.1016/0022-1694(70)90255-6, 1970.

Pietrafesa, L. J., Janowitz, G. S., Chao, T. Y., Weisberg, R. H., Askari, F., & Noble, E.: The physical oceanography of Pamlico Sound. University of North Carolina Sea Grant Publication UNC-WP-86-5, Raleigh, North Carolina, 125, 1986

Pietrafesa, L.J., Bao, S., Yan, T., Slattery, M., Gayes, P.T.: On Sea Level Variability and Trends in United States Coastal Waters and Relationships with Climate Factors, Advances in Adaptive Data Analysis, 7, 1550005, doi: 10.1142/S1793536915500053, 2015.

Pickering, M. D., Wells, N.C., Horsburgh, K. J., and Green, J. A. M.: The impact of future sea-level rise on the European Shelf tides. Continental Shelf Research 35: 1-15, doi:10.1016/j.csr.2011.11.011, 2012.

Sakib, M., Nihal, F., Haque, A., Rahman, M., Ali, M.: Sundarban as a Buffer against Storm Surge Flooding, World Journal of Engineering and Technology, 3, 59, doi: 10.4236/wjet.2015.33C009, 2015.

SMRC.: The Vulnerability Assessment of the SAARC Coastal Region due to Sea Level Rise: Bangladesh Case, SAARC Meteorological Research Center, Dhaka SMRC-No. 3, 2003.

Vatvani, D.K., Gerritsen, H., Stelling, G. S., Rao, A. K.: Cyclone induced storm surge and flood forecasting system for India. Solutions to Coastal Disasters '02, San Diego, CA, 2002.

Warrick, R.A., Bhuiya, A.A.H., Mitchell, W.M., Murty, T.S., Rasheed, K.B.S.: Sea-level Changes in the Bay of Bengal, in: The Implications of Climate and Sea–Level Change for Bangladesh, Springer, pp. 97–142, 1996.

Whitehead, P.G., Barbour, E., Futter, M.N., Sarkar, S., Rodda, H., Caesar, J., Butterfield, D., Jin, L., Sinha, R., Nicholls, R., others.: Impacts of climate change and socio-economic scenarios on flow and water quality of the Ganges, Brahmaputra and Meghna (GBM) river systems: low flow and flood statistics, Environmental Science: Processes & Impacts, 17, 1057–1069, doi: 10.1039/C4EM00619D, 2015.

Xie, L., Bao, S., Pietrafesa, L.J., Foley, K., Fuentes, M.: A real-time hurricane surface wind forecasting model: Formulation and verification, Monthly Weather Review, 134, 1355–1370, doi:10.1175/MWR3126.1, 2006.

Zhang, K., Liu, H., Li, Y., Xu, H., Shen, J., Rhome, J., Smith, T.J.: The role of mangroves in attenuating storm surges, Estuarine, Coastal and Shelf Science 102, 11–23, doi: 10.1016/j.ecss.2012.02.021, 2012.

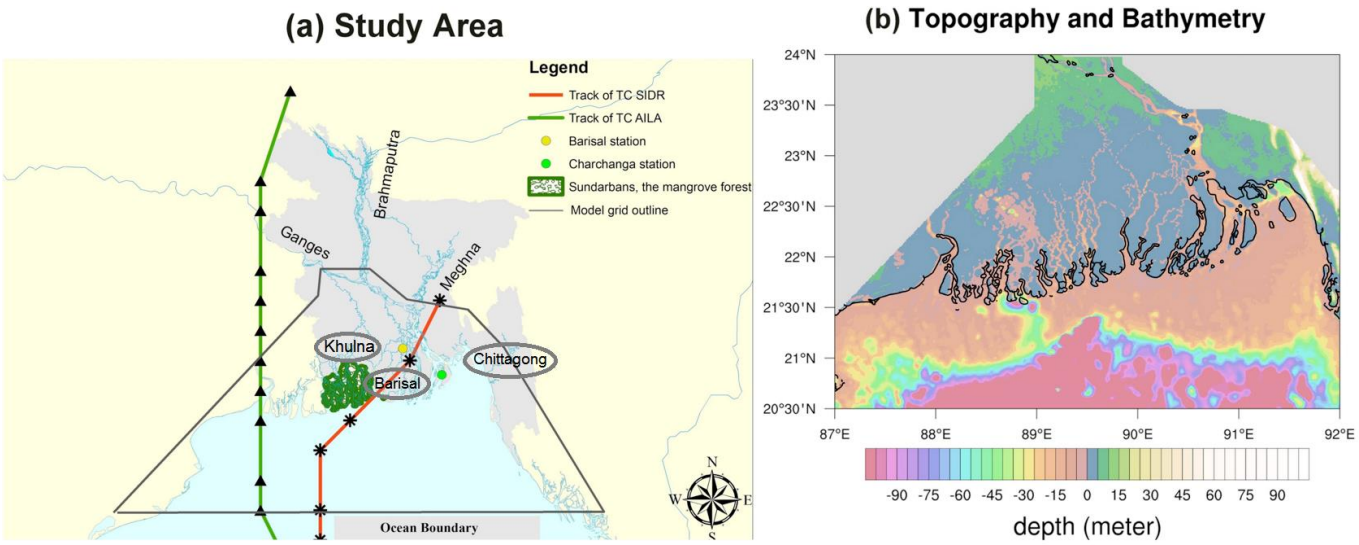

Figure 1. (a) Map of the study area for this work. The red and green lines represent the tracks of TC Sidr and TC Aila respectively. The area marked with green color indicates the Sundarban mangrove forest region. Location of the Ganges, Brahmaputra and Meghna rivers are shown on the map. Khulna, Barisal and Chittagong which are landfall locations for the historical TCs used for ensemble projection, are shown inside a circular box on the map. Two circles over the study area are the observation stations of Bangladesh Inland Water Transport Authority (BIWTA). The black colored outline shows the extent of model grid over the region. (b) Topography and bathymetry of the model domain. Negative depth values represent water bodies (ocean and rivers) and positive depth values areas represent land.

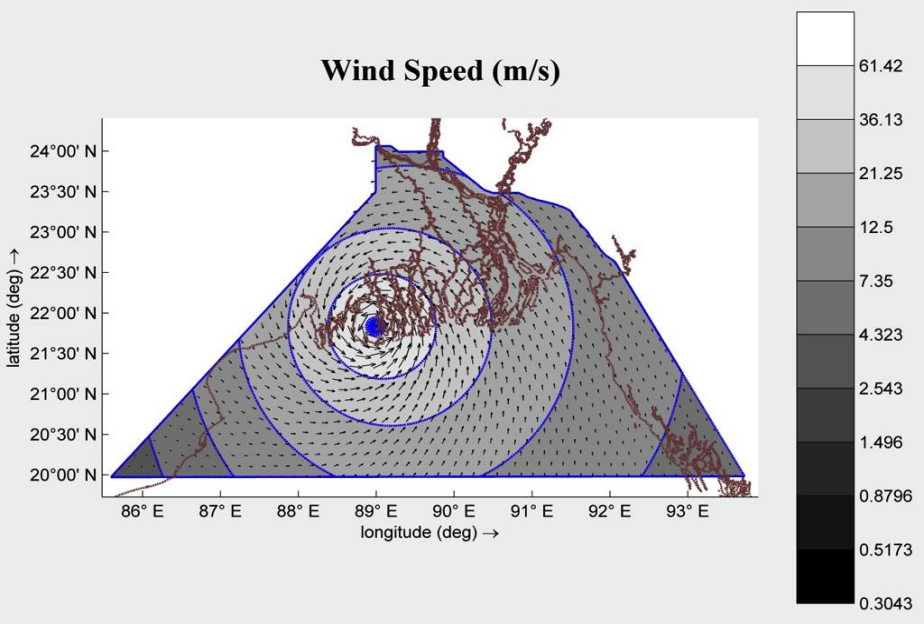

Figure 2. Distribution of the wind field over the model domain for TC Sidr during landfall generated using Holland's Equation.

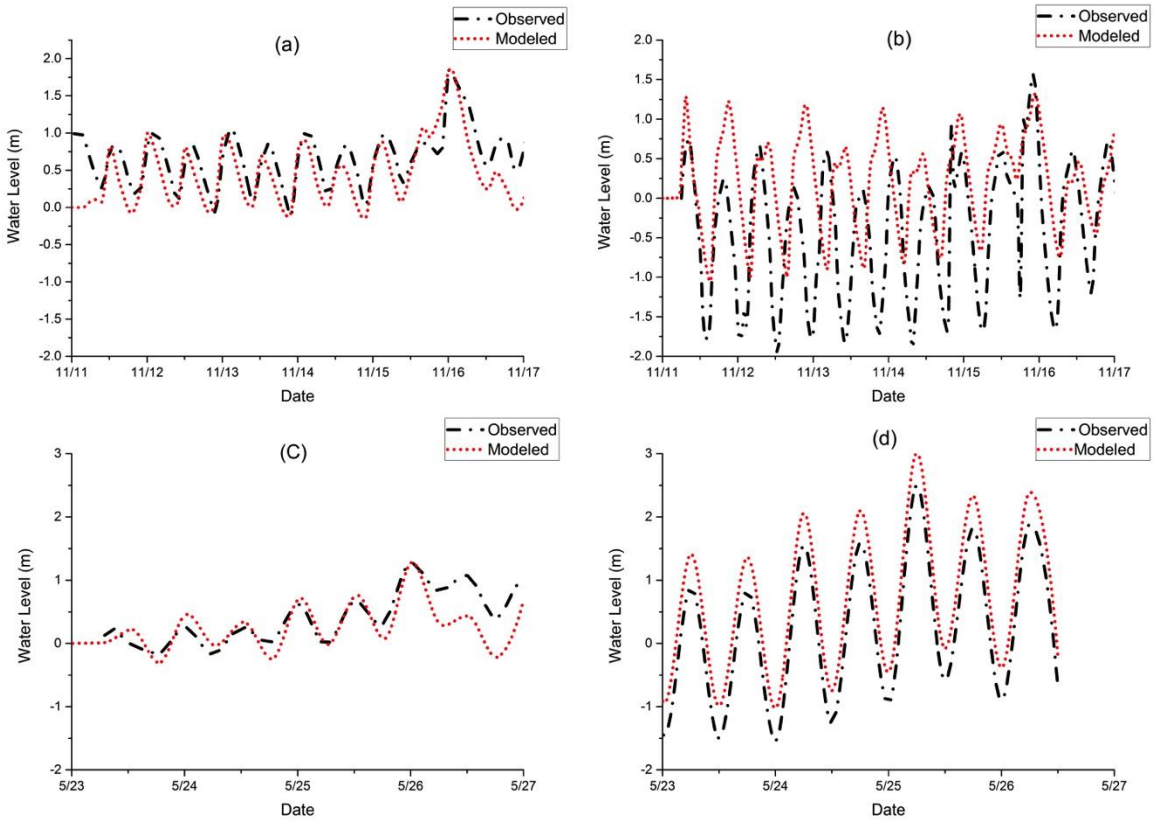

Figure 3. Comparison of observed and modeled water level for TC Sidr and TC Aila in Barisal and Charchanga observation stations. (a) measured and modeled water level comparison for TC Sidr in Barisal (b) TC Sidr in Charchanga (c) TC Aila in Barisal (d) TC Aila in Charchanga.

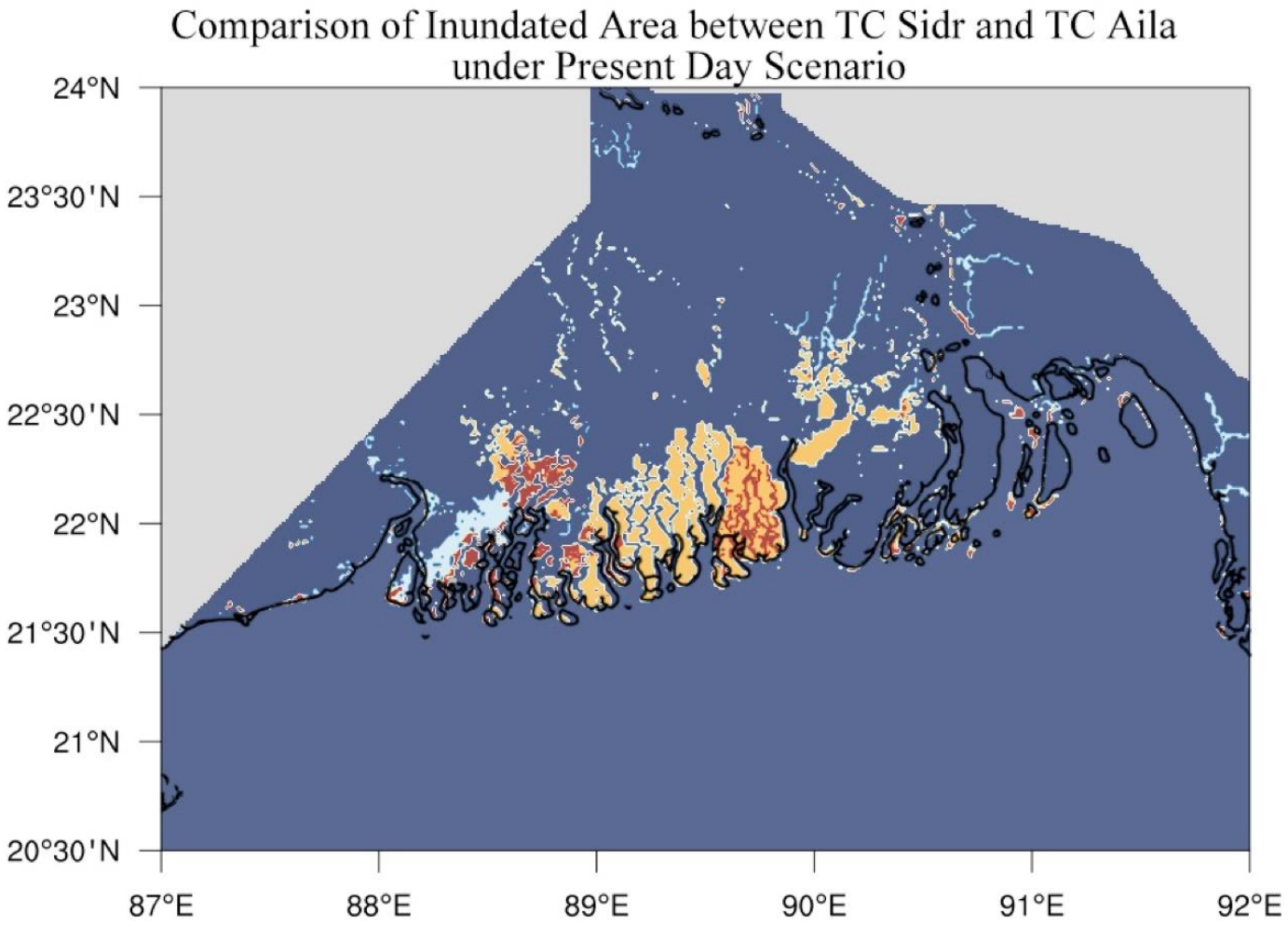

Figure 4. Yellow colors denotes the areas flooded by TC Sidr but not in Aila, and the white color representing the area inundated by TC Aila but not in Sidr. Red color is the area flooded by both TC Sidr and TC Aila. Blue color is showing the non-flooded area (either land or constant water).

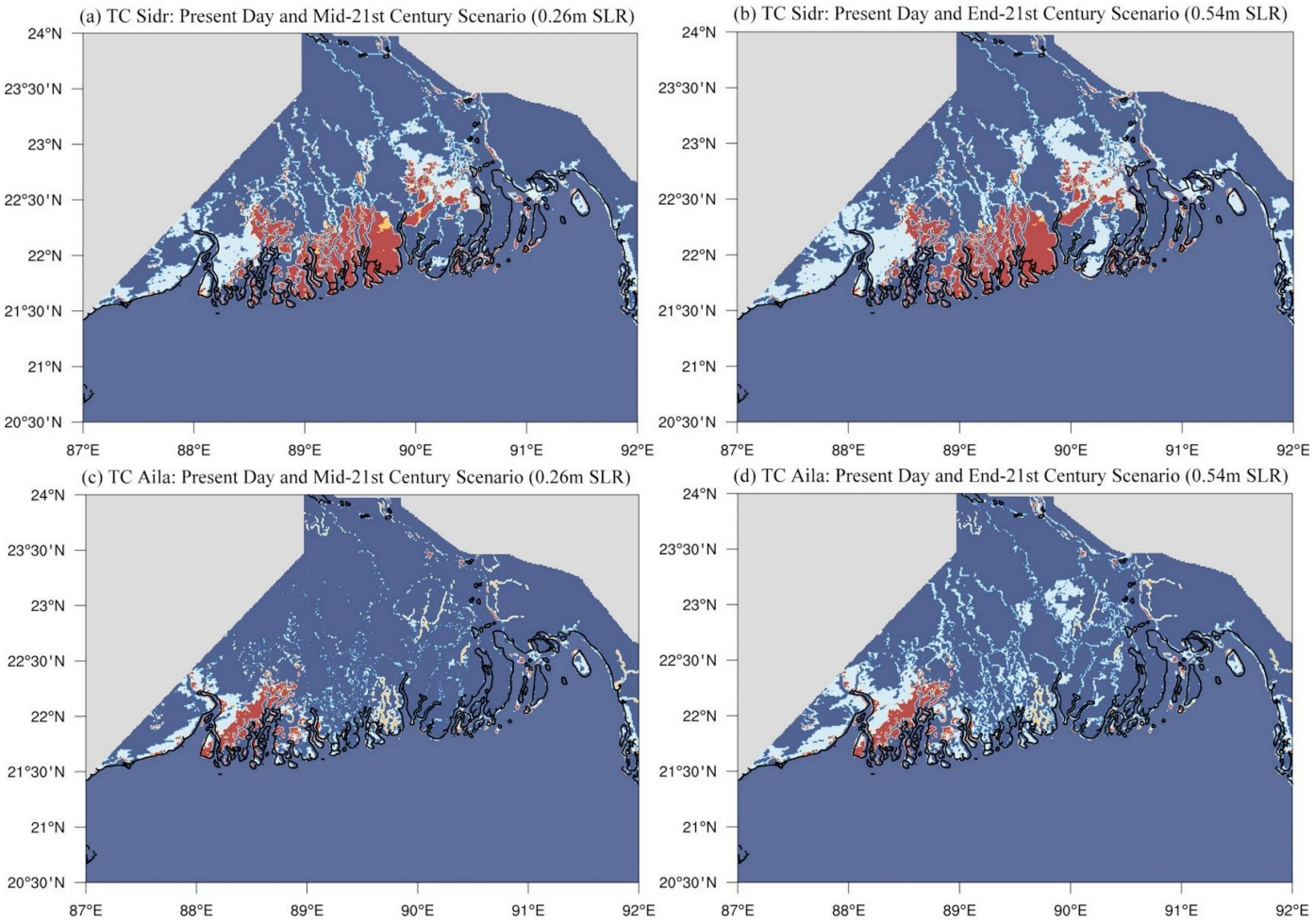

Figure 5: Comparison of inundated area between present-day and future climate scenarios for (a) TC Sidr mid-21st-century 0.26m SLR (b) TC Sidr end-21st-century 0.54m SLR (c) TC Aila mid-21st-century 0.26m SLR (d) TC Aila end-21st-century 0.54m SLR. White color is representing the increased flooded areas that were not in present-day scenario but the increase due to future SLR. Red color is showing the inundated areas that were similar both for present-day and future SLR scenario case.

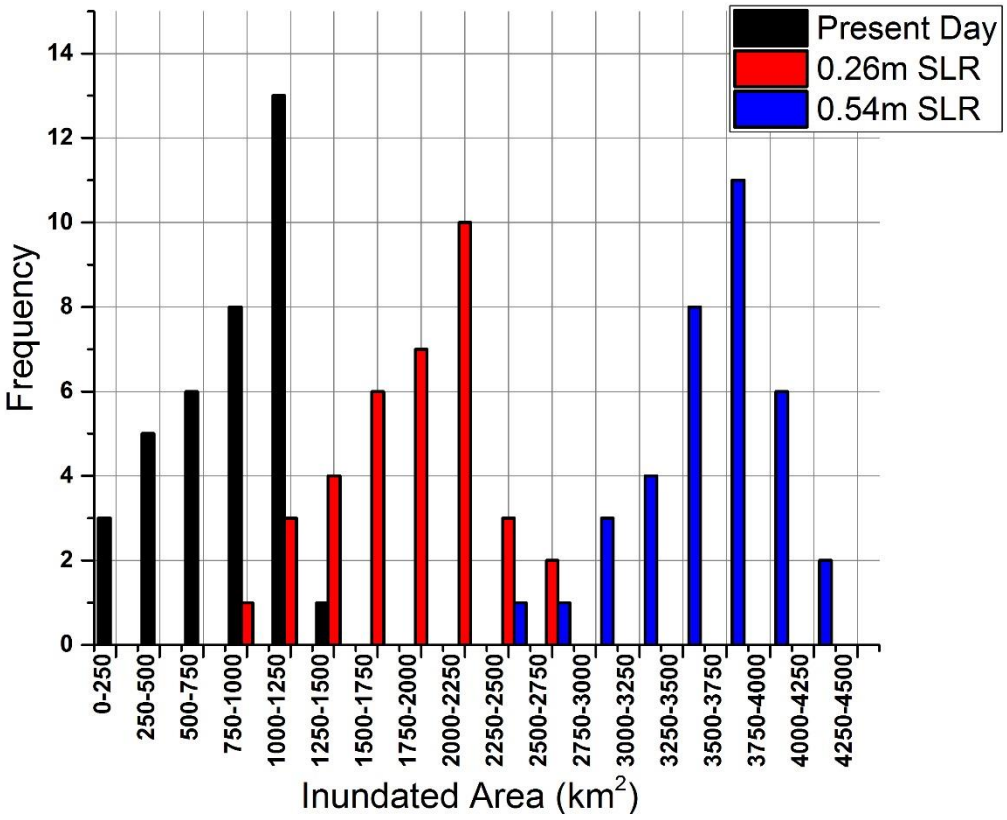

Figure 6: Ensemble projection of the future SLR impact on storm surge inundation. The column in black color is representing the inundation events for present-day sea level condition, red colored one is for 0.26 m of SLR and blue colored column is for 0.54 m of SLR conditions. In total 108 simulations were conducted for present and two future SLR scenarios.

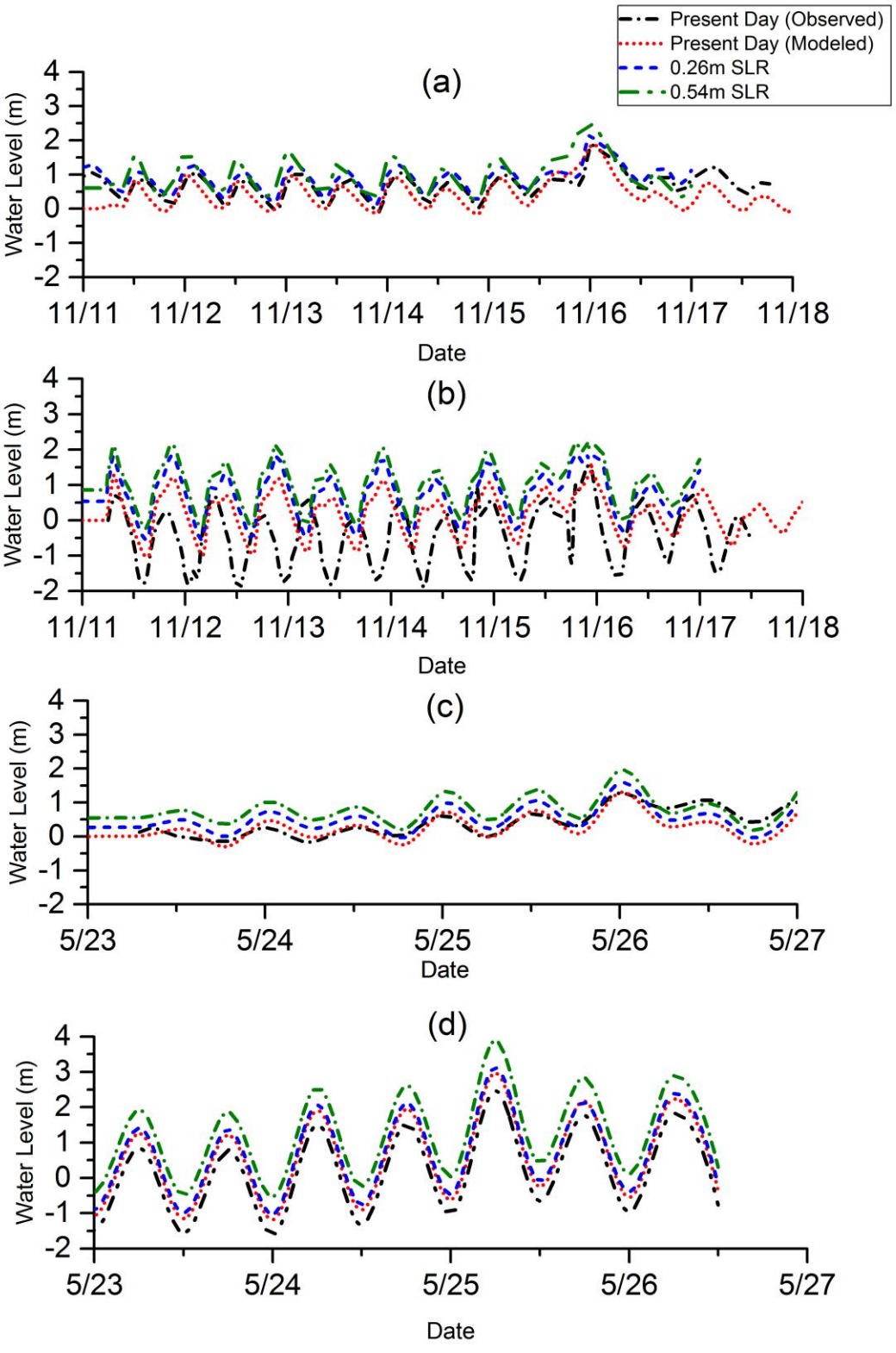

Figure 7. Comparison of storm surge water levels between present-day and future SLR scenarios. (a) TC Sidr at Barisal (b) TC Sidr at Charchanga (c) TC Aila at Barisal (d) TC Aila at Charchanga. The observed, modeled present-day, mid-21st-century and end-21st-century storm surge levels are denoted by the black dash-dotted, red dotted, blue dashed, and green dash-dottted lines, respectively.

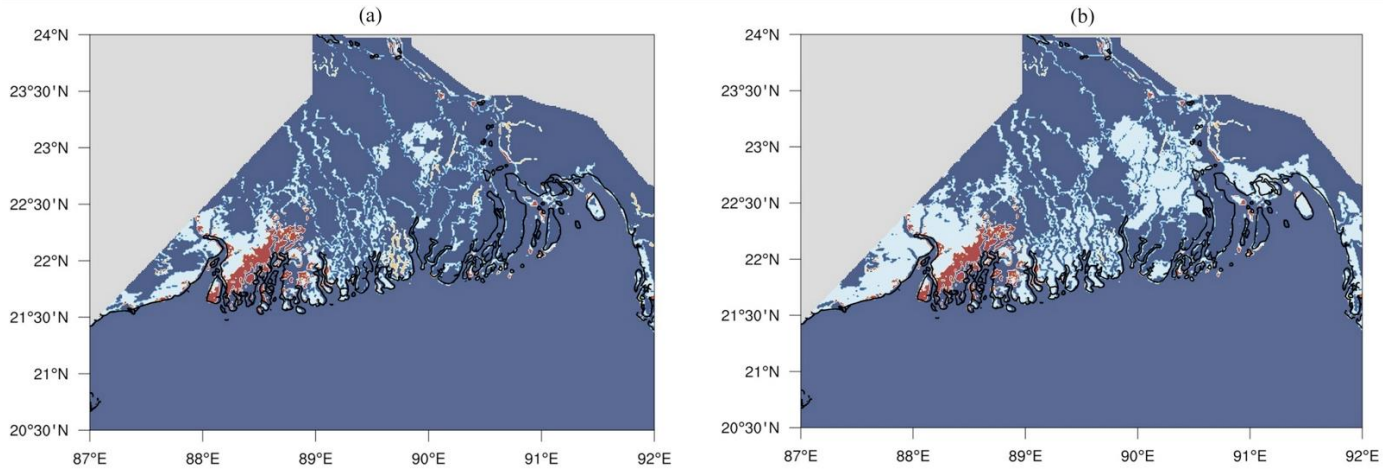

Figure 8. Comparison of inundated areas for TC Aila between present-day and end-21st-century (0.54m SLR) scenario. White color is representing the increased flooded areas that were not in present-day scenario but the increase due to future SLR. Red color is showing the inundated area that's similar both for present-day and future scenario case. Blue areas are either land or constant waters (those which are already water at the model initialization time). Figure (a) is representing the inundated area when SLR was considered on ocean depths instead of adding it in to the open ocean boundary and Figure (b) is showing the inundated area when we considered the SLR on ocean boundary.

Table 1 Manning's Roughness Coefficient for different land coverings.

Land cover	Manning's coefficient
River	0.015
Mangrove	0.080
Ocean	0.01
Land	0.025

Table 2 List of 12 historical TC events used for ensemble projection of storm surge inundation

Name	Date	Landfall location	Maximum sustained wind (km/h)
Tropical storm 13	14-18 November, 1973	Noakhali	102
Cyclone 12	23-28 November, 1974	Bhola	139
Tropical storm 19	07-12 November, 1975	Chittagong	93
Tropical storm 1	22-25 May, 1985	Noakhali	110

Cyclone 4	21-30 November, 1988	Khulna	205
Cyclone 2	22-30 April, 1991	Chittagong	235
Cyclone 2	26 April – 02 May, 1994	Cox's Bazar	215
Cyclone 4	18-25 November, 1995	Cox's Bazar	190
Cyclone 1	13-20 May, 1997	Noakhali	165
Tropical storm 4	24-27 October, 2008	Barguna	85
Tropical storm Mahasen	10-16 May, 2013	Patuakhali	85
Tropical storm Roanu	18-21 May, 2016	Chittagong	110

Table 3: Parameters considered for ensemble projection of storm surge inundation which includes the TC intensities, tidal conditions and the SLR scenarios.

TC name	**Intensities**	**Tide conditions**	**SLR**
TC Sidr	+10%, present day, -10%	high, low, actual, zero	present day, 0.26 m, 0.54 m
TC Aila	+10%, Present day, -10%	high, low, actual, zero	present day, 0.26 m, 0.54 m
12 historical TC tracks	actual intensities	actual	present day, 0.26 m, 0.54 m

Table 4. Computed values of RMSE, MAE and Nash-Sutcliffe coefficient for both TC Sidr and TC Aila

Stations	**TC Sidr**			**TC Aila**		
	RMSE (m)	MAE (m)	NASH	RMSE (m)	MAE (m)	NASH
Barisal	0.23	0.16	0.85	0.33	0.24	0.65
Charchanga	0.26	0.19	0.80	0.28	0.17	0.73

Table 5. Comparison of inundated area between present-day & future SLR scenarios and calculated change in percentage with respect to present-day scenario.

SLR **Scenario**	**TC Sidr**		**TC Aila**	
	Inundated Area (km^2)	**(%) increase**	**Inundated Area (km^2)**	**(%) increase**
present-day	1860	n/a	1208	n/a
mid-21st century	2437	31%	1550	28%
end-21st century	2846	53%	1770	47%

Table 6. Comparison of storm surge level between present day and future SLR scenarios and increase in storm surge level with respect to the present day and SLR scenario for the case of TC Sidr and TC Aila in Barisal and Charchanga observational stations. The SLR scenarios of 0.33 m, 0.40 m and 0.47 m were used to examine the linearity/non-linearity of increase in storm surge level with respect to SLR conditions. In the table "w.r.t" stands for "with respect to".

SLR (m)	TC Sidr						TC Aila					
	Barisal			Charchanga			Barisal			Charchanga		
	surge(m)	increase w.r.t present-day (m) and (%)	increase w.r.t. SLR (%)	surge(m)	increase w.r.t present day (m) and (%)	increase w.r.t. SLR (%)	surge (m)	increase w.r.t. present day (m) and (%)	increase w.r.t. SLR (%)	surge (m)	increase w.r.t present day (m) and (%)	increase w.r.t. SLR (%)
0.00	1.87	n/a	n/a	1.64	n/a	n/a	1.29	n/a	n/a	2.50	n/a	n/a
0.26	2.13	0.26 (14%)	100%	1.87	0.23 (14%)	88%	1.58	0.29 (22%)	112%	3.07	0.57 (23%)	219%
0.33	2.21	0.34 (18%)	103%	1.95	0.31 (19%)	94%	1.66	0.37 (29%)	112%	3.22	0.72 (29%)	218%
0.40	2.26	0.39 (21%)	97%	2.00	0.36 (22%)	90%	1.75	0.46 (36%)	115%	3.42	0.92 (37%)	230%
0.47	2.32	0.45 (24%)	96%	2.08	0.44 (27%)	94%	1.82	0.53 (41%)	113%	3.67	1.17 (47%)	249%
0.54	2.41	0.54 (29%)	100%	2.19	0.55 (34%)	102%	1.96	0.67 (52%)	124%	3.87	1.37 (55%)	254%